Chen et al. *Microsystems & Nanoengineering* (2025)11:147
https://doi.org/10.1038/s41378-025-00985-5

Microsystems & Nanoengineering
www.nature.com/micronano

ARTICLE Open Access

Planar-electroporated cell biosensor for investigating potential therapeutic effects of ectopic bitter receptors

Changming Chen[1,2], Jianguo Wu[1,3], Chunlian Qin[1,4], Yong Qiu[1,3], Nan Jiang[1], Qifei Wang[1], Mengxue Liu[1], Deming Jiang[1,3], Qunchen Yuan[1,3], Xinwei Wei[5]✉, Liujing Zhuang[1,6]✉ and Ping Wang[1,2,3]✉

Abstract

Bitter receptors were initially identified within the gustatory system. In recent years, bitter receptors have been found in various non-gustatory tissues, including the cardiovascular system, where they participate in diverse physiological processes. To investigate the electrophysiological and potential therapeutic implications of bitter receptors, we have developed a highly sensitive, multifunctional planar-electroporated cell biosensor (PECB) for high-throughput evaluation of the effects of bitter substances on cardiomyocytes. The PECB demonstrated the capability for high-throughput, stable, and reproducible detection of intracellular action potentials (IAPs). In comparison to conventional biosensors that utilize extracellular action potentials (EAPs) for data analysis, the IAPs recorded by the PECB provided high-resolution insights into action potentials, characterized by increased amplitudes and an enhanced signal-to-noise ratio (SNR). The PECB successfully monitored IAPs induced by the activation of bitter receptors by using three bitter substances: diphenidol, denatonium benzoate, and arbutin in cardiomyocytes. To further assess the drug development ability of our PECB, we established an in vitro long QT syndrome (LQTS) model to investigate the potential therapeutic effects of arbutin. The results indicated that arbutin altered the electrophysiological properties of cardiomyocytes and significantly shortened the repolarization time in the LQTS model. Moreover, it demonstrated its potential mechanistic pathway by activating bitter receptors to modulate cardiac ion channel activities. The developed PECB provides an effective platform for high-throughput screening of substrates of bitter receptors for the treatment of heart disease, presenting new opportunities for the development of antiarrhythmic therapies.

Introduction

Bitter receptors are integral to mammalian taste perception and were initially identified in taste buds[1]. Interestingly, recent studies have revealed that bitter receptors are also extensively expressed in non-gustatory tissues, including the gastrointestinal tract, respiratory system, and cardiovascular system[2–4]. Most importantly, these ectopically expressed bitter receptors participate in diverse physiological processes[5]. For example, ectopically expressed bitter receptors within the cardiovascular system have been increasingly recognized for their potential role in regulating cardiac physiological functions, including modulating heart rate, rhythm, and contractility[6]. However, the potential therapeutic effects of these ectopic bitter receptors as drug targets in heart disease remain unexplored.

As a potential tool for investigating the potential therapeutic effects of ectopic bitter receptors in heart disease, the patch-clamp technique offers precise IAPs recording and can provide rich information about ion channels on the cell membrane[7,8]. However, its low throughput and lack of long-term monitoring ability are key limitations that hinder its use in drug screening. Because of the non-invasive nature and the convenience of electrode arrangement,

Correspondence: Xinwei Wei (weixinwei@zju.edu.cn) or Liujing Zhuang (zhuangliujing@zju.edu.cn) or Ping Wang (cnpwang@zju.edu.cn)
[1]Biosensor National Special Laboratory, Key Laboratory for Biomedical Engineering of Education Ministry, Department of Biomedical Engineering, Zhejiang University, Hangzhou 310027, China
[2]The MOE Frontier Science Center for Brain Science & Brain-Machine Integration, Zhejiang University, Hangzhou 310027, China
Full list of author information is available at the end of the article
These authors contributed equally: Changming Chen, Jianguo Wu

microelectrode array-based biosensors provide feasible tools for high-throughput drug screening[9–11]. Nevertheless, the EAPs' records are susceptible to interference from neighboring cell signals, affecting signal interpretation and quality. Innovative technologies employing electroporation or optoacoustic approaches have emerged to overcome these constraints. For example, intracellular electrical signals from cardiac cells were able to be recorded by applying electroporation on a three-dimensional nanopillar electrode device with a 4×4 platinum pad array[12]. A 32-channel scalable nano-trap matrix-enhanced electroporation electrode array was designed capable of record primary rat cardiomyocytes' intracellular signals[13]. Dipalo et al. achieved optoacoustic imaging by applying laser pulses to a high-density complementary metal-oxide-semiconductor (CMOS) multi-electrode array, recording intracellular signals from various cells[14]. The necessity for customized and complex micro-nano fabrication methods and the high cost of laser equipment limit the widespread application of these technologies. Therefore, there is an urgent need for a high-throughput and simplified method capable of reliably capturing detailed intracellular electrophysiological signals for effective cardiac drug screening, particularly for evaluating the therapeutic effects of bitter receptors.

Here, using the electroporation technique, we investigated the potential therapeutic effects of ectopic bitter receptors. First, we developed a PECB based on HL-1 cardiomyocytes for the high-throughput evaluation of the therapeutic potentials of bitter substances in heart disease treatment (Fig. 1). The PECB employs standard microfabrication techniques combined with electrode surface modifications using platinum nanoparticles (PtNPs) to establish a nanogranular structure. This approach significantly decreases electrode impedance and enhances electroporation efficiency, allowing stable, reproducible, and high-quality IAPs recording. Compared to EAPs, the IAPs exhibited higher amplitudes and improved SNR, facilitating more precise signal analysis. Then, utilizing the PECB, we evaluated the electrophysiological effects of three representative bitter substances (diphenidol, denatonium benzoate, and arbutin) on HL-1 cardiomyocytes. Furthermore, an in vitro LQTS model was constructed to assess the potential therapeutic effects of arbutin on arrhythmia. Our findings elucidated the potential signaling pathways through which arbutin activates bitter receptors and modulates the electrophysiological activities of cardiomyocytes. This work provides an efficient platform for the screening of prospective cardiac medications.

Materials and methods

Preparation and modification of planar-electroporated cell biosensor

The PECB was fabricated through standard microfabrication of an MEA sensor, coupled with the application of nanoparticles on the working electrodes' surface. The lithography masks required for the MEA sensor were designed by AutoCAD (Autodesk, USA). The MEA sensor was designed in a 12 mm × 12 mm square structure, which was arranged in an 8×8 array with a total of 60 working electrodes. The electrode diameter was 30 μm, and the electrode spacing was 200 μm. A 4-inch, 0.5 mm-thick (SCHOTTAG, Germany) quartz glass slide was used as the device substrate. Lift-off resist (LOR) and AZ5214 double-layer adhesive process were used for lithography and development. The Cr/Au (20 nm/200 nm) electrodes, transfer points, and lead patterns were fabricated by sputtering and lift-off processes. A layer of Si_3N_4 (500 nm) passivation pattern was fabricated by plasma-enhanced chemical vapor deposition (PECVD) for insulation. Reactive ion etching (RIE) was used to expose the electrode and metal transfer points. For the MEA sensor preparation, the MEA chip was fixed on a customized printed circuit board (PCB) adapter by epoxy adhesive (Deli, China), and all metal transfer points were connected to PCB pads using gold wire. Finally, a circular acrylic chamber was glued at the center of the MEA sensor for cell culture by epoxy adhesive (Fig. S1).

For the modification of PtNPs on MEA sensor electrodes, a PtNPs solution (Sigma-Aldrich, USA) was added to the circular acrylic chamber. The electrode on the MEA sensor as the working electrode, the platinum wire counter electrode (CH Instruments, Inc., China), and the Ag/AgCl reference electrode (CH Instruments, Inc., China) were connected to the CHI760E electrochemical workstation (CH Instruments, Inc., China) for electroplating PtNPs. Set the working constant voltage as −0.1 V, the working time as 60 s, and the sensitivity as 10^{-3} A/V. The impedance spectra were used to detect the electrode impedance before and after electroplating based on the CHI760E electrochemical workstation. In the circular acrylic chamber with phosphate-buffered saline (PBS), 5 mV sinusoidal excitation was applied, and the detection interval was 1 Hz–10 kHz.

Culture of HL-1 cardiomyocyte cells

HL-1 cardiomyocytes were used in this study. The medium for culturing HL-1 cardiomyocytes was prepared in advance, consisting of Claycomb medium (Sigma-Aldrich, USA), 10% F8318 fetal bovine serum (Sigma-Aldrich, USA), 1% 10 mM norepinephrine (Sigma-Aldrich, USA), 1% 200 mM L-glutamine (Sigma-Aldrich, USA), 1% 100 U/mL penicillin and 100 μg/mL streptomycin (Thermo Fisher Scientific, USA). The cryopreserved HL-1 cardiomyocyte cell was thawed and placed in a T25 (Corning, USA) culture flask pre-coated with 0.02% gelatin and 5 μg/mL fibronectin solution (Aladdin, China). HL-1 cardiomyocyte cells were cultured in an incubator (37 °C, 5% CO_2). The

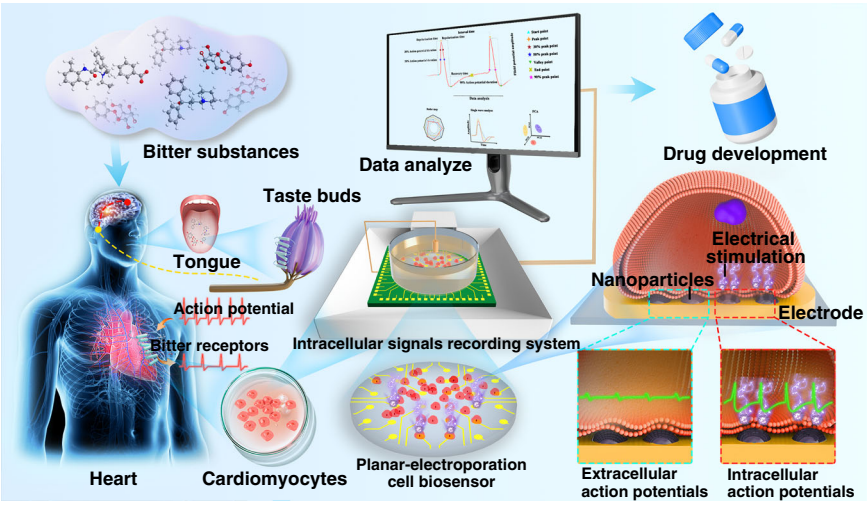

Fig. 1 Schematic diagram of the PECB which evaluates the effects of bitter substances on electrophysiological activities in cardiomyocytes for drug development. Bitter receptors are mainly expressed in the taste system and are also expressed in the heart. The planar-electroporated cell biosensor (PECB) was developed to evaluate the effects of bitter substances on electrophysiological activities and their potential as drugs for heart diseases. HL-1 cardiomyocytes were cultured on the PECB modified with platinum nanoparticles (PtNPs). By applying electric pulses (20 pulses per second), the permeability of the cell membrane was transiently increased, and high-quality and high signal-to-noise ratio (SNR) intracellular action potentials (IAPs) could be recorded without affecting cell viability. The IAPs of HL-1 cardiomyocytes under the action of different bitter substances were further analyzed by feature extraction and data analysis

medium was refreshed every 48 h. After the cells were 100% confluent, the cells were digested with Trypsin-EDTA (Sigma-Aldrich, USA) and seeded into the planar-electroporated cell biosensor at a density of 250,000 cells/well. Cells were passaged every 3-4 days using Trypsin-EDTA and reseeded at the appropriate density. The sensor was sterilized with 75% ethanol and UV light in a biological safety cabinet in advance, and then coated with fibronectin (Sigma-Aldrich, USA) and processed overnight at 4 °C. The planar-electroporated cell biosensor with HL-1 cardiomyocytes was planted in a 37 °C, 5% CO_2 incubator, and the medium was renewed for 48 h. IAPs were recorded on day 3 after seeding on the biosensor surface.

Intracellular action potential recording with electroporation

MEA2100-Lite-System (Multichannel systems, Germany) was used to record HL-1 cardiomyocyte EAPs and cell electroporation for recording IAPs. The PECB with HL-1 cardiomyocytes was placed into the MEA2100 adapter plate with a signal amplifier. An Ag/AgCl-pellet (P1060) reference electrode (Multichannel systems, Germany) was used as the ground line. The device was placed in a 37 °C, 5% CO_2 incubator for long-term recording. The signal was sampled at 10 kHz by a multi-channel experimenter (Multichannel Systems, Germany) software, and filtered with band-pass filtering of 0.1 Hz–10 kHz by hardware. HL-1 cardiomyocytes could generate action potentials spontaneously, producing instantaneous transmembrane potentials and ionic currents, which caused electrode potential changes through the electric double-layer model, and then the extracellular action potential was recorded by electrodes. For the IAPs obtained by electroporation, a 1 s bidirectional pulse electrical stimulation (20 pulses per second) was applied with a pulse width of 200 μs by the MEA2100 pulse generator. The recording of the IAPs was maintained during electroporation. Electrical signal artifacts were generated due to amplifier saturation and were not considered IAPs until the baseline was restored.

Detection of bitter substances

The three bitter substances tested in this study, denatonium benzoate, diphenidol, and arbutin, were purchased from Sigma-Aldrich, USA. Different concentrations of denatonium benzoate (100, 500, 1000, 1500, and 2000 μM), diphenidol (50, 62.5, 78, 125, and 150 μM), and arbutin (10, 30, 50, 70, and 100 mM) were used for detection. The concentrations were selected with reference to the reported literature[15]. Before each bitter substance detection, electroporation was performed to record a section of IAPs as the control signal of this experiment. After adding bitter substances, electroporation was performed to record the IAPs stimulated by bitter substances. Then the PECB was washed three times with PBS to elute bitter substances, and new medium was used to replace the old medium mixed with bitter substances.

Construction of LQTS model and evaluation of its therapeutic effects by bitter substances

LQTS is a heart condition where delayed repolarization in heart cells leads to a prolonged QT interval on an electrocardiogram. We utilized E-4031, a specific IKr current blocker, which prolongs the repolarization time of cardiomyocyte action potentials by inhibiting K^+ channels, thereby simulating LQTS arrhythmia models in vitro[16]. Initially, the optimal concentration of E-4031 was selected to establish the in vitro LQTS model, first recording a segment of IAPs from normal cardiomyocytes as control signals. Following the addition of E-4031, the samples were incubated for 30 minutes before re-recording the IAPs of the cardiomyocytes post-intervention. The criterion for constructing the in vitro LQTS model was a significant extension of the repolarization time of the IAPs. The arbutin was employed as a potential therapeutic agent for LQTS, introducing it in concentrations of 10, 30, 50, 70, and 100 mM into the established in vitro LQTS model, followed by a 30-minute incubation period to evaluate its effects on repolarization time. Afterward, the PECB was rinsed three times with PBS to remove E-4031 and arbutin, and fresh medium was introduced to replace the previously used medium containing the bitter substance.

Data analysis and statistics

Detailed data analysis methods, including IAPs feature extraction, normalized signal analysis, and SNR calculation methods, have been provided in Supplementary Methods S9. The principal component analysis (PCA) method was used to analyze the features[17]. All results were expressed as mean ± standard deviation (SD). Data were analyzed using GraphPad Prism 8 (GraphPad Software Inc., USA) for data analysis. Multiple comparisons were performed using ordinary one-way ANOVA to calculate p-values. Significance was set at 0.05 for most tests, with significance levels defined as follows: $^{*}p < 0.05$, $^{**}p < 0.01$, $^{***}p < 0.001$, $^{****}p < 0.0001$, ns, not significant.

Results

Establishment and characterization of planar-electroporated cell biosensor

Figure 2a shows the physical image of the PECB, which consists of an MEA sensor and a transfer PCB. A transparent acrylic chamber is affixed to hold the medium necessary for cell culture. The MEA sensor in Fig. 2b was designed as an 8 × 8 array, consisting of 60 working electrodes with a diameter of 30 μm and an inter-electrode spacing of 200 μm. The microfabrication process of the proposed PECB is comprehensively described in Fig. S1. The surface of the gold electrode was electrochemically modified with PtNPs (Fig. 2d), resulting in a reduction of the electrode impedance (Fig. 2c). Scanning electron microscope (SEM) images of the electrode, before and after modification, are presented in Fig. 2e and Supplementary Methods S1. Before modification, the surface of the gold electrode appeared smooth (Fig. 2e (i), (ii)). After modification, the surface was decorated with PtNPs, forming a nanogranular structure (Fig. 2e (iii), (iv)). Figure 2f shows the results of immunofluorescence staining detailed in supplementary methods S2, which indicate that HL-1 cardiomyocytes cultured on the sensor expressed typical cardiomyocyte markers (α-actinin and cardiac troponin I (cTnI)). The presence of the culture medium did not significantly affect the baseline measurements (Fig. S2a, b). Although the HL-1 cell culture introduced some background noise, the effective signal amplitude was significantly higher than the baseline (Figs. S2a, b and 2h). Similarly, buffer solution injection resulted in a transient noise spike that rapidly subsided and did not interfere with the overall signal recording (Fig. S2c). The PECB was placed in a 37 °C, 5% CO_2 incubator for recording (Fig. S3).

Electroporation is a technique that enhances cell membrane permeability to facilitate the recording of intracellular signals through the application of electrical stimulation[18]. The electrical stimulation parameters were optimized to achieve accurate and stable intracellular signal recordings from HL-1 cardiomyocytes. A range of stimulation amplitudes was tested using 200 μs biphasic pulses (20 Hz, 1 s), including 0.5, 1, 2, and 3 V, to assess the impact of electroporation amplitude on cellular viability and the quality of recorded intracellular signals. Figure 2g shows the results of live/dead staining after electroporation with an electrical stimulation amplitude parameter of 1 V (Supplementary Methods S3). Specific electrodes were selected for electroporation (Fig. 2g (i), white arrows), and a magnified view of one electrode demonstrated that the cells remained viable after electroporation (Fig. 2g (ii)). These results confirmed that the 1 V electroporation parameter does not compromise the viability of HL-1 cardiomyocytes. Meanwhile, the typical extracellular signals recorded (Fig. 2h (i-ii)) were consistent with the EAPs reported in previous studies[19], indicating that HL-1 cardiomyocytes were well-adhered to the electrodes and exhibited spontaneous rhythmic activity. Figure 2h (iii) illustrates the electrical signals recorded after electroporation at 1 V. After electroporation, typical intracellular signals were observed, which were significantly distinct from the EAPs (Fig. 2h (iv)). Over time, these intracellular signals gradually reverted to the characteristic shape of EAPs. In addition, these post-electroporation EAPs (Fig. 2h (v)) showed no significant differences when compared to pre-electroporation EAPs (Fig. 2h (ii)), indicating that the 1 V electroporation parameter did not affect the cells' intrinsic

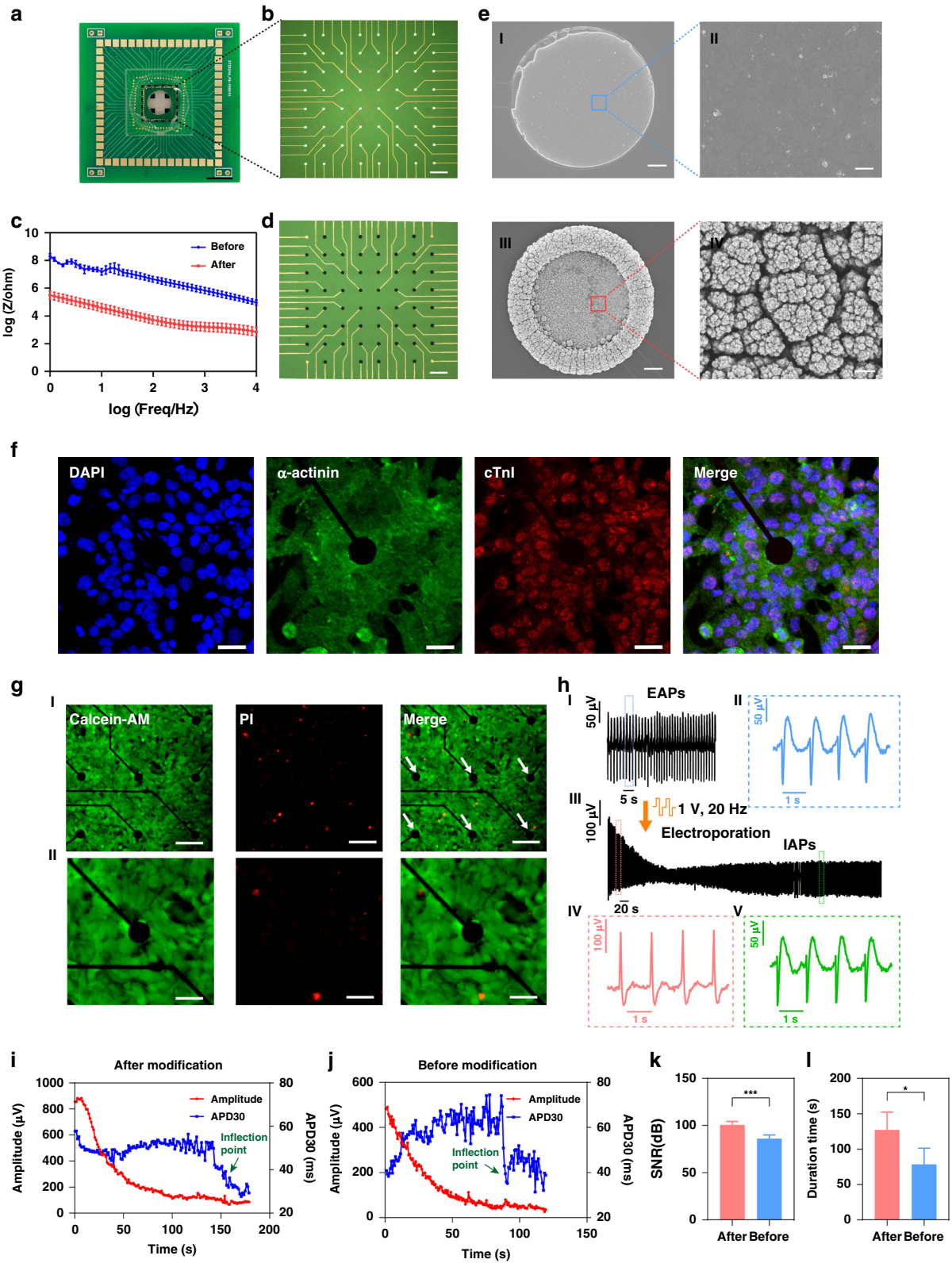

Fig. 2 (See legend on next page.)

(see figure on previous page)

Fig. 2 Establishment and characterization of the PECB. a Physical view of the PECB. The black dashed box shows the MEA sensor. Scale bar = 1 cm. **b** Microscope image of the sensor with the 8 × 8 array layout of the electrodes (without modification). Scale bar = 200 μm. **c** The electrode impedance curve before and after modification. **d** Modified electrodes with PtNPs. Scale bar = 200 μm. **e** SEM images of the electrode before and after modification. (i-ii) The smooth surface of the unmodified electrode. Scale bars = 5 μm. (iii-iv) Nanogranular structure surface of modified electrodes. Scale bar = 200 nm. **f** Immunofluorescence staining for DAPI (blue), α-actinin (green), and cTnI (red) in cardiomyocytes. Scale bars = 30 μm. **g** Live/dead staining after electroporation with an optimized voltage of 1 V. (i) Comparison of the cell viabilities with and without electroporation. Live cells are marked using Calcein-AM (green) while dead cells are marked using PI (red). White arrows show the electroporated electrodes. Scale bars = 200 μm. (ii) Zoomed-in image of a single electrode after 1 V electroporation. Scale bars = 50 μm. **h** Spontaneous signals of HL-1 cardiomyocytes before and after 1 V electroporation. (i) A segment of recorded extracellular signals. (ii) The extracellular signals were typical EAPs of HL-1 cardiomyocytes. (iii) A segment of recorded signals after 1 V electroporation. (iv) The typical intracellular signals after electroporation. (v) The signals were restored into EAPs after electroporation at 1 V. **i**, **j** The statistical analysis of amplitude and APD30 of signals from electrodes before and after modification. **k** The statistical analysis of SNR before and after modification ($n = 5$). **l** The statistical analysis of duration time before and after modification ($n = 5$)

electrophysiological properties. In contrast, at lower voltage (0.5 V), intracellular signals were not detectable, whereas increased voltages (2 and 3 V) resulted in irreversible cellular damage, leading to cell death and an inability to revert normal EAPs, as detailed in Fig. S4. Consequently, the optimal electrical stimulation parameter for electroporation in detecting intracellular signals was determined to be 1 V. This optimal parameter was subsequently applied to deliver the membrane-impermeable calcein dye into HL-1 cells (Supplementary Methods S4, Fig. S5), further confirming that the electroporation was successful and the recorded signals originated from intracellular electrophysiological activity, consistent with previous study[12]. Notably, fluorescence staining results demonstrated that the intracellular signals were exclusively recorded from cells on the electrodes, thereby minimizing potential interference from neighboring cells.

To investigate the influence of PtNPs modification on electroporation efficiency, we compared the intracellular signals recorded using modified and unmodified biosensors. Visualization of the intracellular signals' amplitude and the 30% action potential duration (APD30) over time revealed that the modified biosensor sustained a higher signal amplitude for a prolonged period, with a longer duration of APD30 before reaching the inflection point (Fig. 2i, j). The decrease of APD30 represented the transition from intracellular signals to EAPs, thus, the inflection point of APD30 was employed to determine the duration of intracellular signals. Further statistical analysis of the SNR and intracellular signals duration for both modified and unmodified sensors (Fig. 2k, l) indicated that the modified sensor exhibited a higher SNR (100.70 ± 1.38 dB) compared to the unmodified sensor (86.16 ± 1.96 dB). Moreover, the duration of intracellular signals recorded by the modified sensor (127.2 ± 12.58 s) was significantly longer than that of the unmodified sensor (78.49 ± 13.25 s). These results demonstrated that the PtNPs modification effectively enhances electroporation efficiency.

Intracellular action potentials recording of HL-1 cardiomyocytes by planar-electroporated cell biosensor

In the experiments described above, the PECB was demonstrated to record intracellular signals effectively. The intracellular signals needed further verification as IAPs. As shown in Fig. 3a, the blue signal represents the spontaneous EAPs signals from HL-1 cardiomyocytes. Intracellular signals were recorded after applying the optimized electrical stimulation (red). Figure 3b presents a segment of EAPs and intracellular signals. Before electroporation, the recorded signals displayed signatures of extracellular characteristics, including a short-duration spike with lower amplitudes (Fig. 3b (i), (iv)). After electroporation, the spike amplitude and waveform exhibited a dramatic change toward a larger positive phase (Fig. 3b (ii), (v)), resembling the shape of IAPs recorded by patch-clamp[20]. The signal had a characteristic cardiomyocyte action potential waveform, including depolarization, repolarization, and resting phases. To verify the composition of the recorded intracellular signals, an equivalent circuit model of the cell-electrode interface was established (detailed in Supplementary Methods S5). The model demonstrated that electroporation significantly reduced cell membrane impedance and temporarily increased membrane permeability, enabling the recording of intracellular signals consistent with IAPs. Comparing the first derivative of the intracellular signal (Fig. 3b (vi)) with the recorded single EAPs (Fig. 3b (iv)) and simulation results (Fig. S6) showed a consistent shape, which further provides that the recorded intracellular signals were IAPs, confirming that the PECB successfully recorded accurate IAPs signals by electroporation[21]. EAPs might exhibit waveform variations due to interference from nearby cells, while IAPs showed more consistent profiles, allowing for enhanced feature extraction in the analysis of bitter substances (Fig. 3c). Further analysis demonstrated that the amplitude of the IAPs (791.6 ± 148.0 μV) was significantly higher than the amplitude of the EAPs (176.0 ± 16.1 μV). Moreover, the SNR of the IAPs (106.1 ± 1.8 dB) exceeded that of the EAPs (86.0 ± 1.5 dB), indicating that the IAPs

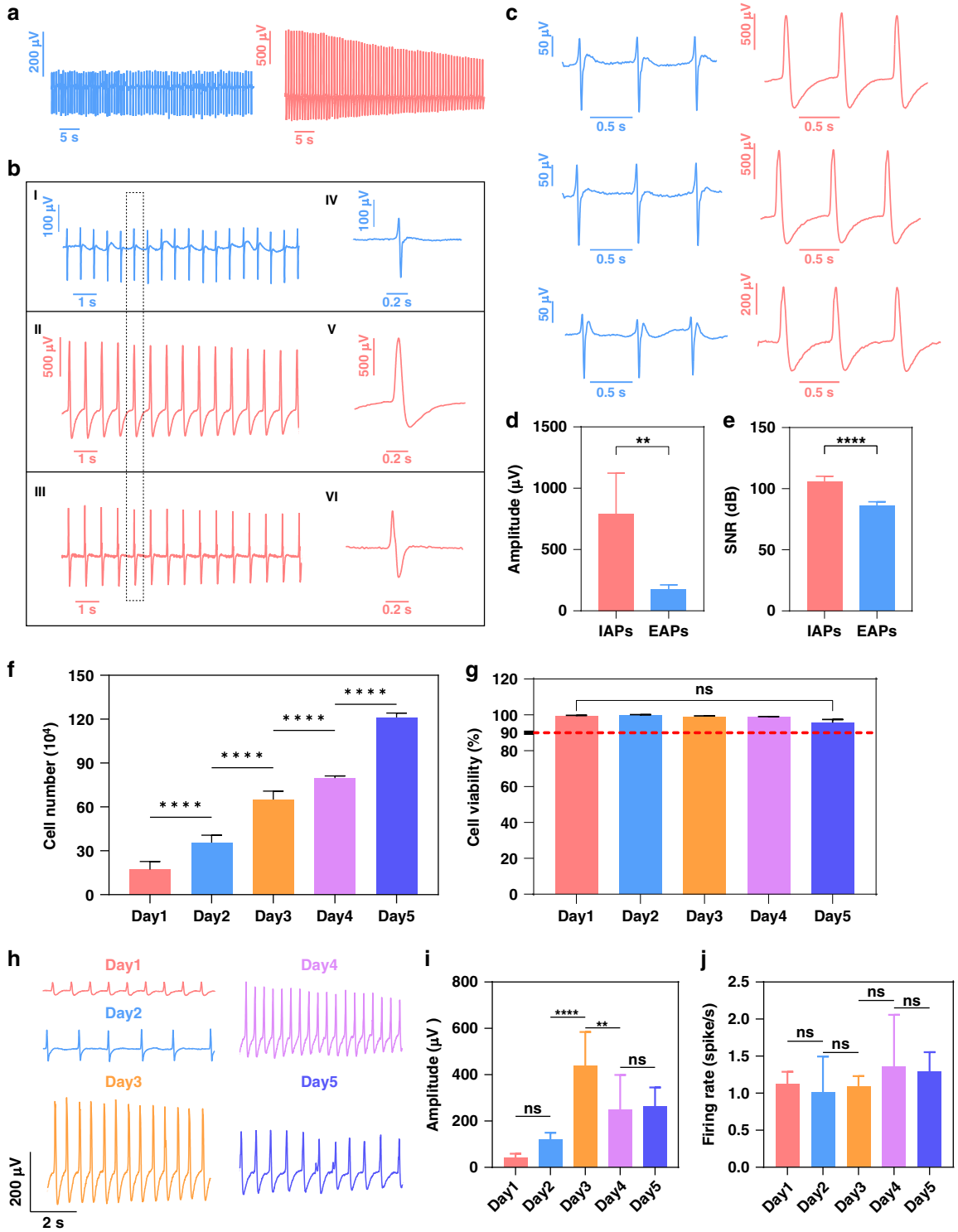

Fig. 3 Characterization of IAPs recorded after electroporation and biocompatibility of the PECB. a The representative signals of EAPs (blue) and intracellular signals (red) of HL-1 cardiomyocytes. **b** The representative signals of EAPs and intracellular signals, and the data calculated by a first-derivative method based on the intracellular signals. The intracellular signals were verified as intracellular action potentials (IAPs). (i, iv) The segment of typical EAPs and a typical spike of EAPs. (ii, v) The segment of typical intracellular signals and a typical spike of intracellular signals. (iii, vi) The data calculated by a first-derivative method based on the intracellular signals and a typical spike. **c** Typical EAPs (blue) and IAPs (red) of HL-1 cardiomyocytes were recorded by PECB. **d** The statistical analysis of amplitudes of EAPs and IAPs ($n = 5$). **e** The statistical analysis of the SNR of EAPs and IAPs ($n = 5$). **f** The statistical analysis of the cell number cultured on the PECB from day 1 to day 5. **g** The statistical analysis of cell viability with high cell viability (>90%). **h** The typical IAPs recorded in culture for 1 to 5 days. **i** The statistical analysis of the amplitude of recorded IAPs for 1 to 5 days ($n = 5$). **j** The statistical analysis of the firing rate of recorded IAPs for 1 to 5 days ($n = 5$)

with PECB could significantly improve signal quality and provide high-resolution details of cardiomyocyte action potentials compared to the EAPs (Fig. 3d, e).

The stability of IAPs under the 1 V parameter was evaluated through continuous recordings following electroporation (Fig. S7). As shown in Fig. S7b, the IAPs amplitude initially reached 1299.67 μV (i, 10 s), then gradually decreased to 961.02 (ii, 30 s), 753.41 (iii, 50 s), 647.03 (iv, 70 s), 533.11 (v, 90 s), and 490.31 μV (vi, 110 s). This amplitude reduction reflected an increase in cell–electrode interface impedance as the cell membrane recovers, consistent with our equivalent circuit model (Fig. S6b). Despite the reduction in amplitude during this period, the IAPs waveform remained unchanged, indicating a stable shape throughout the recording period. To quantify these observations, we performed statistical analyses of the amplitude and APD90 over multiple IAPs recordings (Fig. S7c, d). The amplitudes decreased from 1335.00 ± 10.26 (10 s) to 188.90 ± 3.48 (110 s), while the APD90 varied slightly from 890.00 ± 2.97 (10 s) to 933.70 ± 18.34 ms (110 s), respectively. These results confirm that, although the amplitude decreased over time, the shape and duration of the IAPs remained stable for at least 110 s under the 1 V parameter. Furthermore, the IAPs were maintained after 10 consecutive electroporation cycles (Fig. S8), further demonstrating the robust stability and repeatability of the PECB.

Biocompatibility assessment of planar-electroporated cell biosensor

To assess the biocompatibility of the PECB, HL-1 cardiomyocytes were cultured on the sensor for 5 days. As shown in Fig. S9, the cells grew progressively from Day 1 to Day 5 and fused after Day 3. Cell proliferation assessments using the CCK-8 assay (Fig. S10, Supplementary Methods S6) revealed a significant increase in cell number over this period (Fig. 3f), indicating favorable biocompatibility of the PECB. This was further confirmed by live/dead staining results shown in Fig. S11. During the culture period, the majority of HL-1 cardiomyocytes were stained with Calcein-AM, while only a small fraction was stained with propidium iodide (PI). Additionally, the live and dead cells were quantitatively counted to accurately determine cell viability, which remained above 90% throughout the 5 days (Fig. 3g). In parallel, the IAPs were recorded daily (Fig. 3h). The amplitude of the IAPs increased from 40.36 ± 6.70 μV on day 1 to a maximum of 438.10 ± 51.77 μV on day 5, then decreased to 264.50 ± 23.18 μV by day 5 (Fig. 3i), suggesting that cell density influenced the amplitude and shape of recorded IAPs. Notably, the recorded IAPs no longer exhibited clear single waveforms on day 5. Instead, they showed significantly reduced amplitudes accompanied by irregular waveforms, which might be caused by electrical interference from neighboring cells. However, the firing rates of the IAPs for days 1 through 5 were 1.12 ± 0.06, 1.01 ± 0.18, 1.10 ± 0.05, 1.36 ± 0.26, and 1.28 ± 0.09 spikes/s respectively, with no significant differences observed during the 5 days (Fig. 3j). These results suggest that cell proliferation might not affect the rhythm of electrophysiological activity but impact the amplitude and shape of IAPs recordings. This effect may arise from reduced cell–electrode coupling and lower sealing resistance as cell density increases (Fig. S6b). Based on these observations, subsequent experiments were performed on day 3 to minimize the influence of cell proliferation on IAPs recording.

Capability of the planar-electroporated cell biosensor to detect changes in IAPs under different bitter substances

Bitter substances have been reported in previous studies that could activate bitter receptors (T2Rs) in the cardiomyocytes, leading to changes in ion channels on the cell membrane and altering the action potential of cardiomyocytes[22]. Although the precise signaling mechanisms remain under investigation in cardiomyocytes, two primary signal transduction pathways have been proposed for T2Rs activation, as illustrated in Fig. 4a: Gβγ- phospholipase Cβ2 (PLCβ2)/ inositol 1,4,5-trisphosphate (IP3) and Gαgust- phosphodiesterase (PDE)- cyclic adenosine monophosphate (cAMP)[23]. Upon activation by bitter ligands, the T2Rs coupled to G proteins dissociate into Gαgust and Gβγ subunits[24]. The Gβγ subunit then activates PLCβ2, leading to hydrolysis of phosphatidylinositol 4,5-bisphosphate (PIP2) into IP3 and diacylglycerol (DAG). IP3 stimulates IP3 receptor (IP3R3) to mediate sarcoplasmic reticulum release of Ca^{2+}, increasing intracellular Ca^{2+} concentrations. Elevated intracellular Ca^{2+} modulates calcium-dependent cardiac ion channels, thereby influencing cardiac electrophysiology, particularly by shortening or prolonging action potential duration[25–27]. Furthermore, the Gαgust activates PDE, leading to a reduction in intracellular cAMP levels, and thus inhibits cardiac contraction by attenuating L-type Ca^{2+} channels and the consequent Ca^{2+} release[25]. Consequently, this signaling cascade can change cardiac action potential characteristics[22,28].

The constructed PECB was employed to evaluate the effects of bitter substances on IAPs in HL-1 cardiomyocytes. To explore the expression of bitter receptors in HL-1 cardiomyocytes, we evaluated the mRNA levels of 35 bitter receptors by quantitative reverse transcription PCR (RT-qPCR) (Fig. 4b, Supplementary Methods S7, Table S1). Many T2Rs genes were found expressed in HL-1 cardiomyocytes, including T2R108, T2R126, T2R137, T2R135, T2R140, and T2R144. Based on the bitter gene expression results, three typical bitter substances were selected. Specifically, diphenidol was chosen for its ability

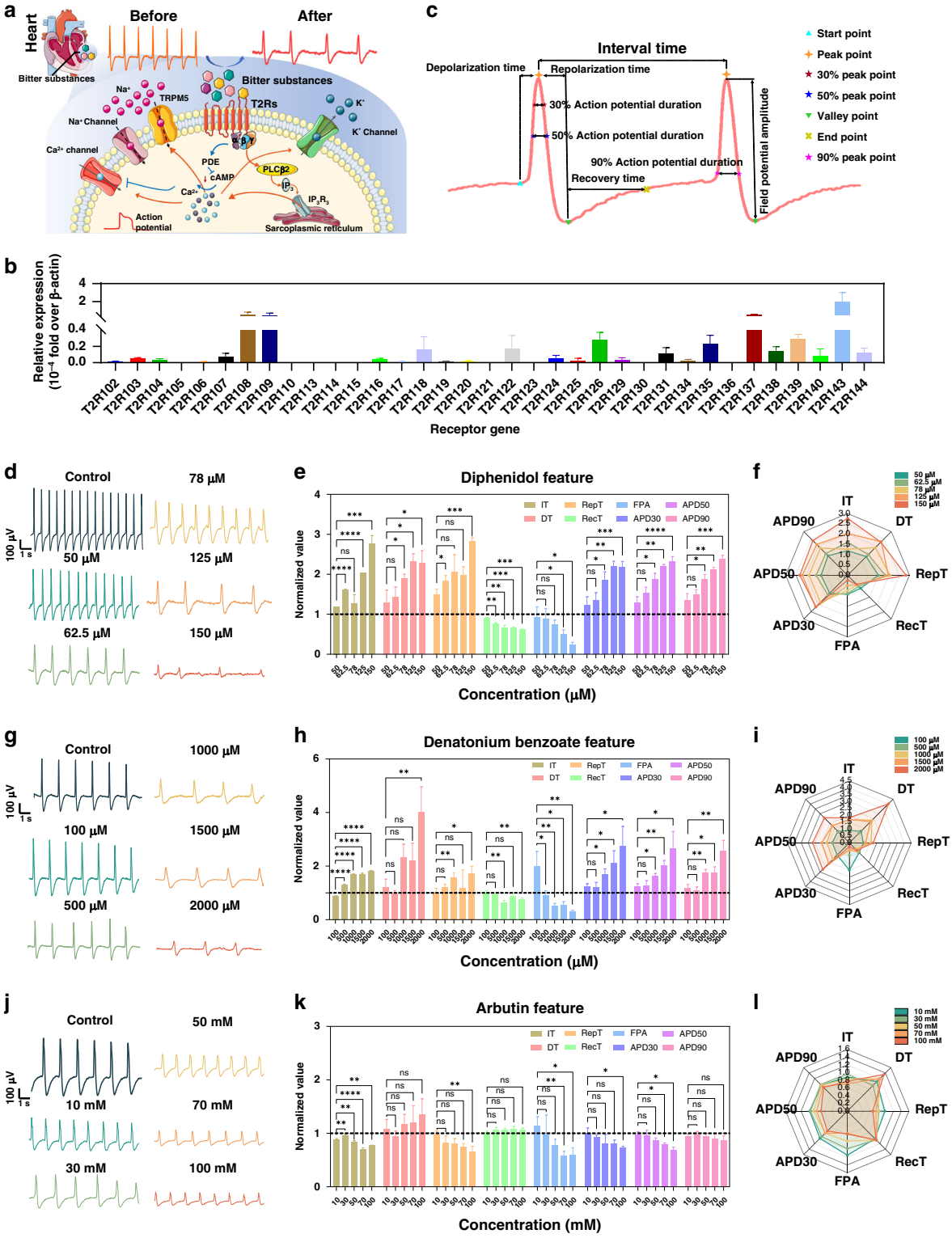

Fig. 4 (See legend on next page.)

(see figure on previous page)

Fig. 4 The effects of different types and concentrations of bitter substances on the IAPs of HL-1 cardiomyocytes by PECB. a Potential signal transduction pathway of bitter receptor (T2Rs) activated by bitter substances in cardiomyocytes. **b** mRNA level of T2Rs (mean fold over β-actin) in HL-1 cardiomyocytes ($n = 3$). **c** Selection of feature points and calculation of feature value. The interspike interval time (IT), depolarization time (DT), repolarization time (RepT), recovery time (RecT), field potential amplitude (FPA), 30% action potential duration (APD30), 50% action potential duration (APD50), and 90% action potential duration (APD90) were extracted as the feature of the IAPs for further analysis. **d**, **g**, **j** Typical IAPs of cardiomyocytes respond to different concentrations of diphenidol, denatonium benzoate, and arbutin, respectively. **e**, **h**, **k** Normalized statistics visualizing 8 extracted features of IAPs under diphenidol, denatonium benzoate, and arbutin, respectively ($n = 5$). **f**, **i**, **l** Radar map visualizing 8 extracted features of IAPs under diphenidol, denatonium benzoate, and arbutin, respectively ($n = 5$)

to activate T2R108, T2R137, and T2R144[15]. It has been reported to suppress the amplitude of action potentials and reduce the firing rate of cardiomyocytes, likely through modulation of cardiac Na^+ channels, and it exhibits antiarrhythmic properties[29,30]. Denatonium benzoate activates T2R135, T2R140, and T2R144, and is reported to attenuate cardiomyocyte excitability and firing rate in a dose-dependent manner[15,31]. In addition to its electrophysiological effects, short-term administration has been shown to downregulate apoptosis and autophagy-related genes, suggesting a potential cardioprotective role[25]. Arbutin was selected for its specific activation of T2R126 and its previously reported effects in reducing pro-inflammatory cytokines and oxidative stress in the myocardium[15,32]. Furthermore, recent studies support its influence on cardiac electrophysiology properties[22]. Therefore, we selected these three bitter substances to evaluate the capability of the PECB to detect IAPs changes induced by T2Rs activation and highlight the potential applicability in novel cardiac drug development.

For further analysis of the IAPs, the 8 features of the recorded IAPs were defined, including the interspike interval time (IT), depolarization time (DT), repolarization time (RepT), recovery time (RecT), field potential amplitude (FPA), APD30, 50% action potential duration (APD50), and 90% action potential duration (APD90) (Fig. 4c). These features were selected based on their ability to reflect distinct physiological phases of the cardiac action potential. Specifically, IT and FPA reflect the rhythmicity and electrical strength of cardiomyocytes[33]. DT, RepT, and RecT represent the temporal properties of different action potential phases, indicating the activation and recovery of ion channels[34]. APD30, APD50, and APD90 provide graded measurements of action potential duration times[35]. To minimize the impact of cell membrane recovery on the recorded IAPs, we limited the analyzed data window to 30 s in the experiment. Figure 4d illustrates the typical IAPs of HL-1 cardiomyocytes at different concentrations of diphenidol. The normalized feature maps and radar map (Fig. 4e, f) showed that as diphenidol concentration increased, the depolarization time was significantly prolonged, accompanied by an increase in the interspike interval time and a decrease in the amplitude of the IAPs. These observations suggested that diphenidol had a potential inhibitory effect on Na^+ channels, consistent with previous studies[29,30]. In addition, APD30, APD50, and APD90 increased substantially at higher concentrations, indicating that diphenidol could prolong the duration of the IAPs. Denatonium benzoate significantly prolonged the interspike interval time of IAPs, thereby slowing their firing rate and reducing their amplitude. These findings are similar to previous studies on the effects of denatonium benzoate on extracellular signals[31]. Further analysis indicated that denatonium benzoate exerted a concentration-dependent influence on depolarization time and the duration of action potentials in HL-1 cardiomyocytes (Fig. 4g–i). By contrast, arbutin displayed different effects on HL-1 cardiomyocytes compared to the other two bitter substances. As the concentration increased, arbutin significantly reduced the interspike interval of IAPs without markedly affecting depolarization time. Instead, it significantly shortened the repolarization time, with a decrease in APD30 and APD50. This indicated that arbutin effectively reduced the duration of the action potential in HL-1 cardiomyocytes (Fig. 4j–l). PCA of the 8 features extracted from three different bitter substances further proved that the selected features could effectively characterize IAPs signals and had the ability to distinguish the types and concentrations of bitter substances (Fig. S12). This suggests that the selected features capture key electrophysiological characteristics of IAPs and can reliably reflect the dose-dependent effects of T2Rs activation. In summary, the PECB could enable quantitative detection of various types and concentrations of bitter substances' effects on IAPs in cardiomyocytes.

Screening of potentially bitter substances for LQTS treatment

LQTS is a cardiac electrophysiological abnormality that may lead to arrhythmias, syncope, and even sudden cardiac death. It is characterized by a prolonged QT interval on the electrocardiogram, which primarily manifests in cardiomyocytes as an extended repolarization time[36]. As mentioned above, we found that arbutin could shorten the repolarization time and the duration of the IAPs in HL-1 cardiomyocytes. Therefore, the potential application of PECB was evaluated to screen arbutin as a potential cardiac

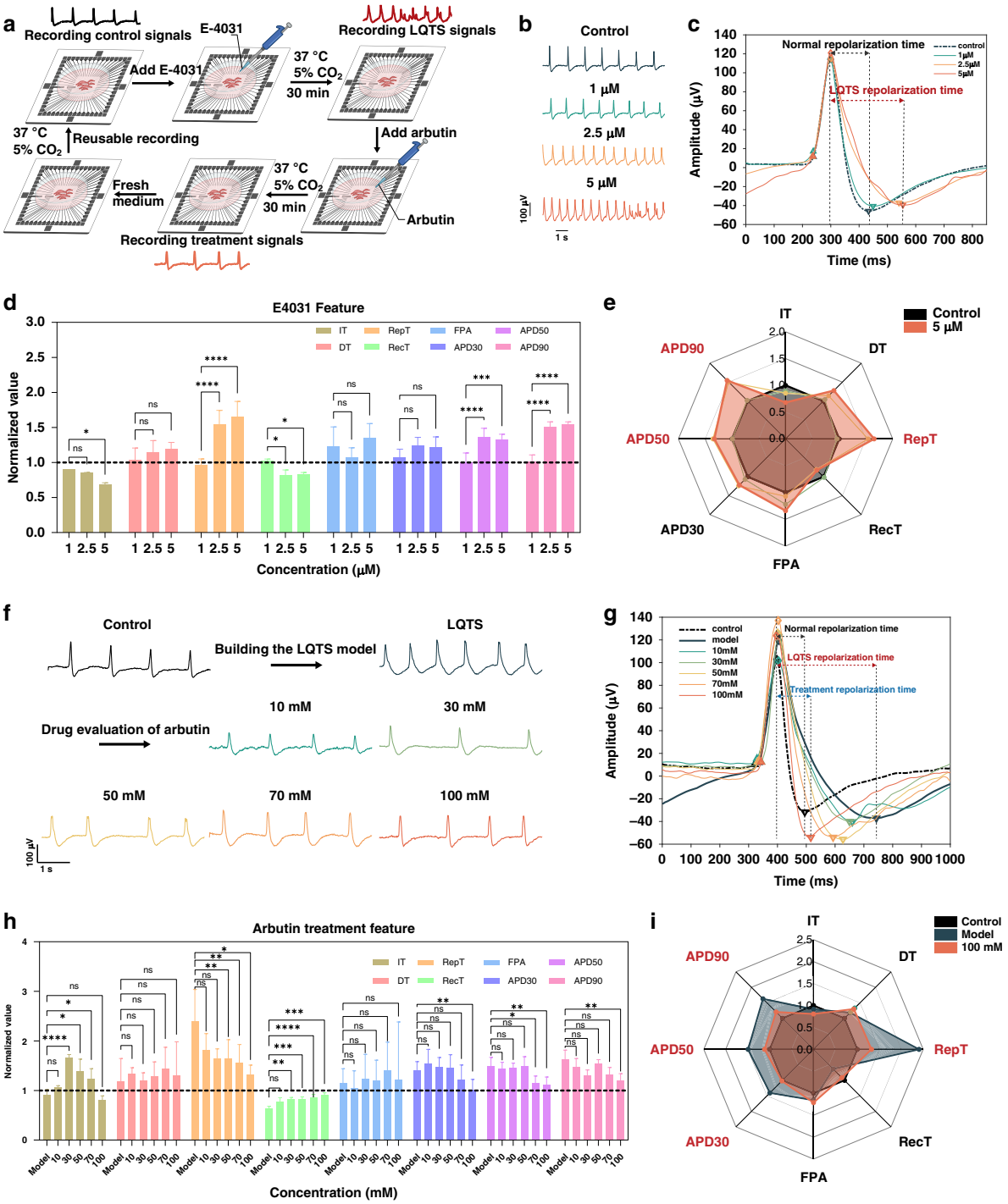

Fig. 5 Construction of the in vitro LQTS arrhythmia model and evaluation of the therapeutic effect of arbutin. a Flow chart of the experiment to evaluate the therapeutic effect of arbutin on the in vitro LQTS model. **b** Typical IAPs of cardiomyocytes responded to different concentrations of E-4031. **c** The average of single IAPs at different concentrations of E-4031 ($n = 5$). **d** Normalized statistics of 8 extracted features for different concentrations of E-4031 ($n = 5$). **e** Radar map of 8 extracted features for different concentrations of E-4031 ($n = 5$). **f** Typical IAPs of cardiomyocytes with different concentrations of arbutin treatment in the LQTS model. **g** The average of single IAPs after treatment with different concentrations of arbutin. ($n = 5$). **h** Normalized statistics visualizing 8 extracted features of IAPs after treatment LQTS model with different concentrations of arbutin ($n = 5$). **i** Radar map visualizing 8 extracted features of IAPs after treatment LQTS model with different concentrations of arbutin ($n = 5$)

drug for the treatment of LQTS. The process of the experiments was conducted by introducing different concentrations of arbutin into the in vitro LQTS model to assess its therapeutic effects on the LQTS, as detailed in Fig. 5a.

Initially, the E-4031 was added to the culture medium of HL-1 cardiomyocytes grown on the PECB to inhibit the K^+ channels within the cardiomyocytes. This intervention was designed to extend the repolarization time of the cardiac action potentials, thereby constructing an in vitro model of LQTS (Fig. 5a). Concentrations of 1, 2.5, and 5 μM E-4031 induced a dose-dependent prolongation in repolarization time, as shown by representative IAP recordings (Fig. 5b). Notably, apparent arrhythmic events occurred when the concentration reached 5 μM. Individual IAPs extracted from continuous recordings (Fig. 5c) illustrated that normal IAPs (126.22 ± 18.84 ms repolarization time) were prolonged to 242.36 ± 181.64 ms at 5 μM E-4031. Further analyses revealed a significant, concentration-dependent increase in repolarization time and marked prolongation of APD50 and APD90 (Fig. 5d, e), confirming the successful construction of the in vitro LQTS model.

Next, different concentrations of arbutin were used to treat the LQTS model (Fig. 5f). With increasing concentrations of arbutin, repolarization times were progressively restored. Visualization of individual IAPs, as shown in Fig. 5g, revealed that the repolarization time of IAPs in normal cells was 116.56 ± 20.37 ms, while the LQTS model showed a significantly prolonged repolarization time of 316.07 ± 155.64 ms. After treatment with 100 mM arbutin, the repolarization time was significantly reduced to 128.58 ± 22.12 ms, showing no statistically significant difference from the repolarization time observed in normal cardiomyocytes ($p > 0.05$). Statistical analysis (Fig. 5h, i) further confirmed these findings, demonstrating that the normalized repolarization time in the LQTS model (2.41 ± 0.63) was significantly reduced to 1.32 ± 0.19 after 100 mM arbutin treatment. Furthermore, the values of APD30, APD50, and APD90 (1.02 ± 0.21, 1.11 ± 0.16, and 1.20 ± 0.14, respectively) were also significantly decreased, with no statistically significant differences compared to the normal cardiomyocytes ($p > 0.05$). These data suggested that arbutin effectively shortened the repolarization time and the duration of action potentials in cardiomyocytes within the LQTS model, thereby mitigating the LQTS. In summary, these results demonstrated that PECB provided a valuable platform for rapidly screening bitter substances as potential cardiac drugs, illustrating its utility in pharmacological evaluations.

Planar-electroporated cell biosensor for exploring mechanisms of ectopic bitter receptors

The potential of arbutin to treat LQTS was investigated by modulating IAPs repolarization time and duration through the activation of ectopically expressed bitter receptors on HL-1 cardiomyocytes. However, the specific mechanism by which these ectopically expressed bitter receptors regulate the membrane ion channels remains unclear. The Na^+, K^+, and Ca^{2+} channels located on the cardiomyocyte membrane are primarily involved in the depolarization and repolarization processes of cardiac electrophysiology. Using the designed PECB, we explored the potential mechanisms of ectopic bitter receptors with arbutin. The results in Fig. 5 demonstrated that arbutin significantly shortened the repolarization time of cardiomyocytes, a process primarily regulated by Ca^{2+} ions. Consequently, it is hypothesized that the activation of bitter receptors by arbutin may influence Ca^{2+} ions dynamics, thereby leading to a reduced repolarization time in cardiomyocytes. To address this, we employed a Ca^{2+}-sensitive light-addressable potentiometric sensor (LAPS) to detect the extracellular fluid Ca^{2+} concentration of HL-1 cardiomyocytes. The LAPS is a field-effect semiconductor biosensor which features a doped silicon substrate with an insulating SiO_2 layer coated by a calcium-ion-sensitive membrane (Supplementary Method S8, Fig. S13). The changes in extracellular Ca^{2+} concentration shift the photocurrent−bias voltage (I-V) curve through surface potential alterations (Fig. 6a). Indeed, Fig. 6b illustrates the I-V characteristic curves of the extracellular fluid in cardiomyocytes under different concentrations of arbutin. The localized magnified view highlighted the region with the greatest gradient on the I-V curve, which showed a gradual rightward shift of the I-V curves with increasing arbutin concentrations, suggesting a corresponding reduction in extracellular Ca^{2+} concentration. Further statistical analysis of photocurrent changes revealed a significant increase from 52.77 ± 31.79 nA at 10 mM to 280.40 ± 32.79 nA at 100 mM (Fig. 6c), confirming that arbutin significantly reduces extracellular Ca^{2+} concentration, indicating the influx of Ca^{2+} ions. These LAPS results provide ionic-level validation of the electrophysiological changes detected by the PECB and support the proposed mechanism that arbutin modulates cardiac repolarization via bitter receptor–mediated Ca^{2+} signaling.

Although not definitively validated, some studies also suggested that bitter receptors may activate protein kinase C (PKC), thereby influencing the Ca^{2+} signaling[37,38]. We further hypothesized a potential transduction pathway, Gβγ-PLCβ2-PIP2-DAG-PKC, which affected Ca^{2+} channels (Fig. 6d). To further validate this pathway, the PECB was utilized with Bisindolylmaleimide I (Bisi), a PKC inhibitor, to inhibit PKC signaling. By examining the IAPs of control, 100 mM arbutin treatment, and 100 mM arbutin with 5 μM Bisi treatment, we observed that inhibition of PKC counteracted the arbutin-induced shortening of the repolarization time (Fig. 6e). Statistical

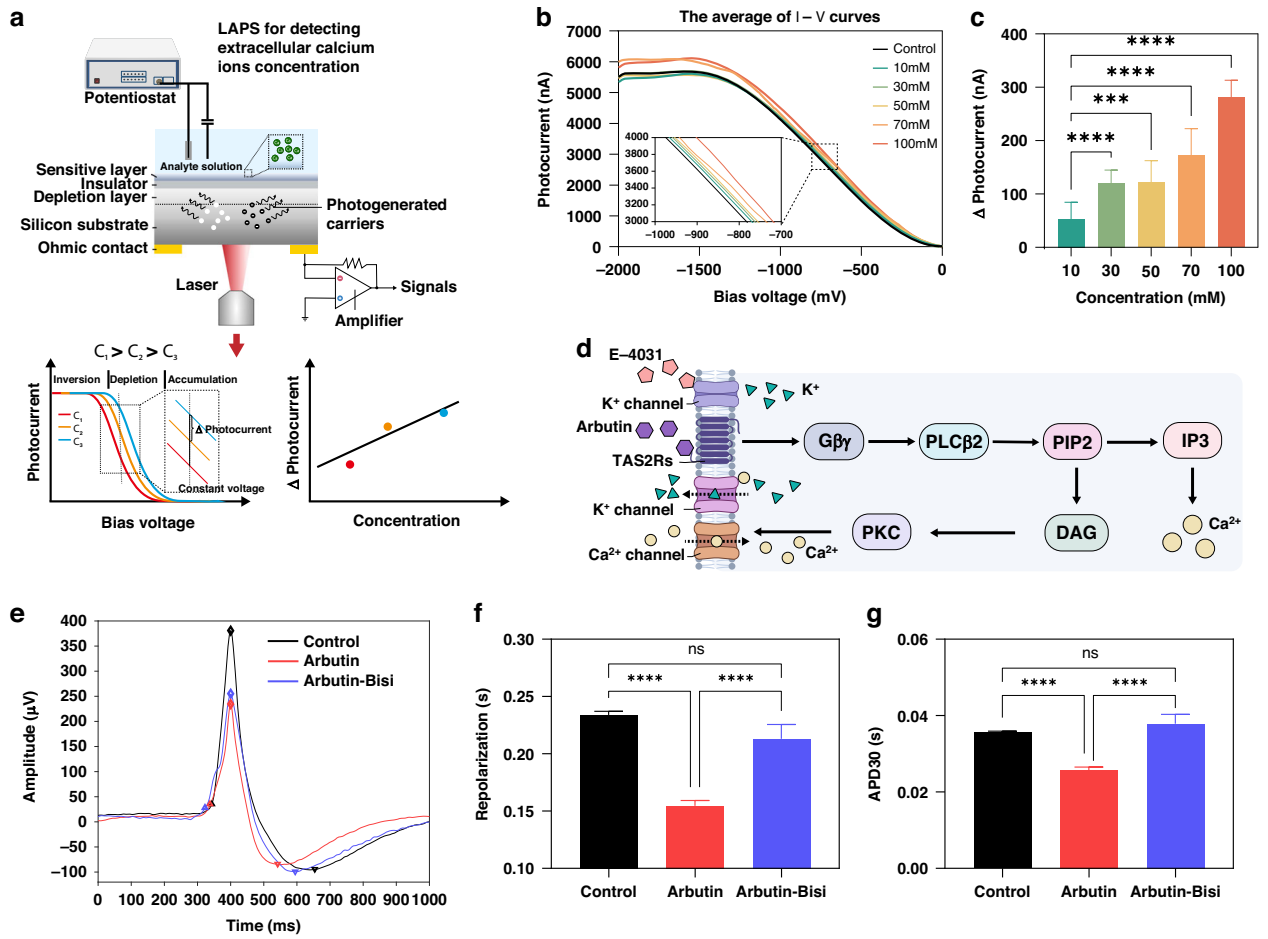

Fig. 6 Exploring mechanisms of ectopic bitter receptors by LAPS and PECB. a Principle of Ca^{2+} ion detection by the calcium-ion-sensitive light-addressable potentiometric sensor (LAPS). A silicone-rubber ion-sensitive membrane modified on the surface of the SiO_2 insulator layer is used as the Ca^{2+}-sensitive material. A direct current (DC) bias applied to the reference electrode (RE) establishes a depletion region at the insulator interface. Selective binding of Ca^{2+} to the membrane induces a change in surface potential, thereby modulating the charge state at the insulator surface. Focused laser illumination generates photogenerated carriers within the insulator substrate, producing a measurable photocurrent. Variations in extracellular Ca^{2+} concentrations result in shifts of the photocurrent–voltage (I–V) characteristics. By recording these photocurrent shifts, quantification of the Ca^{2+} concentration can be achieved. **b** The average of photocurrent—bias voltage (I – V) curves of the calcium-ion-sensitive LAPS with the different concentrations of arbutin ($n = 3$). **c** Photocurrent statistics results of treatment with different concentrations of arbutin ($n = 3$). **d** Hypothesized a potential transduction pathway, Gβγ-PLCβ2-PIP2-DAG-PKC-Ca^{2+} channel. **e** The average of single IAPs before and after PKC channel inhibition with Bisi treatment under 100 mM arbutin ($n = 10$). **f** The statistical analysis of repolarization time was derived from recorded IAPs using PECB, with and without PKC channel inhibition ($n = 10$). **g** The statistical analysis of APD30 derived from recorded IAPs using PECB, with and without PKC channel inhibition ($n = 10$)

analysis further indicated that Bisi could inhibit the reduction in repolarization time and APD30 caused by the bitter substance arbutin, with no significant differences compared to the control (Fig. 6f, g). These findings collectively supported the hypothesis that arbutin might activate PKC, thereby affecting Ca^{2+} to shorten the repolarization time and duration of IAPs. This validation effectively demonstrated that using the PECB could measure and analyze these electrophysiological changes in cardiomyocytes, which would provide a potential application for exploring the signaling mechanisms of ectopically expressed bitter receptors in cardiomyocytes.

Discussion

Ectopic expression of bitter receptors has been implicated in diverse physiological processes, including cardiac function[27]. Although the precise role of bitter receptors in the heart is not yet fully understood, existing evidence suggests that they may contribute to the regulation of cardiac electrophysiology and contractility[15,23]. Thus, these receptors hold significant potential as novel therapeutic targets for cardiac pharmacotherapy. However, there is a notable deficiency in methodologies for rapid and effective evaluation of the therapeutic potential of cardiac ectopic bitter receptors. To address this, we have

developed the PECB, an easy-to-fabricate and high-throughput platform for the recording of IAPs in cardiomyocytes. The PECB integrates PtNPs on planar electrodes to form a nanogranular structure, which is straightforward to fabricate yet effectively reduces impedance and enhances electroporation efficiency (Fig. 2c, i–l), thereby enabling high SNR IAPs recordings. Notably, the platform has 64 channels and achieved stable IAPs recording over 10 cycles per channel without compromising cell viability (Fig. 3c–e, Figs. S7–S8). These showcase the high-throughput, reproducible, and stable features of the PECB.

The PECB facilitated the detailed characterization of intracellular ion alterations resulting from ectopic activation of bitter receptors, thereby enabling the evaluation of their therapeutic potential as drug targets in cardiomyocytes and the investigation of their underlying mechanisms. Arbutin was found to significantly enhance prolonged repolarization times and restore normal action potential duration in IAPs of cardiomyocytes, demonstrating its therapeutic potential for treating arrhythmias. As a proof of concept, the PECB was employed to construct an in vitro LQTS model to evaluate the therapeutic potential of arbutin, and arbutin successfully alleviated symptoms of LQTS. Furthermore, we proposed a potential mechanism for the treatment of LQTS with arbutin, involving the regulation of Ca^{2+} influx. Specifically, arbutin may activate PKC signaling to modulate Ca^{2+} influx, thereby reducing the repolarization time of HL-1 cardiomyocytes. This hypothesis was further validated by recording IAPs using the PECB while inhibiting PKC signaling, consistent with findings from previous studies[37,38].

Utilizing the PECB platform, the impacts of another two bitter substances (diphenidol and denatonium benzoate) on electrophysiological activity in HL-1 cardiomyocytes were also explored. Diphenidol has been reported to depress the action potentials amplitude and decrease the spontaneous firing rates of cardiomyocytes, exhibiting antiarrhythmic properties[29,39]. Diphenidol was found to prolong action potential durations (APD30, APD50, and APD90), reduce IAP amplitudes, and decrease firing rates (Fig. 4d–f), suggesting its potential application in arrhythmia regulation. Furthermore, research has demonstrated that low-dose, short-term treatment with denatonium benzoate led to a reduction in the expression of apoptosis and autophagy-related genes, suggesting its therapeutic potential for cardiac protection[25]. Denatonium benzoate also appears to have the capacity to regulate arrhythmias, as it significantly prolonged depolarization time and the action potential duration while reducing action potential amplitudes and spontaneous firing rates in HL-1 cardiomyocytes (Fig. 4g–i), consistent with a previous study[31].

Compared with nanofabrication-based sensors, such as nanopillar, nanobranch, and nanotrap electrode arrays (Table S2), the PECB was fabricated using standard microfabrication and electrochemical modification techniques, which allow for higher-throughput recording of IAPs. Furthermore, the electroporation approach employed by the PECB for IAPs recording presents a more straightforward approach than optoporation[14], requiring only the application of electrical stimulation. When compared to sensors specifically designed for bitter receptor studies (Table S2), the PECB (30 seconds) had a faster response time than most existing sensors[31,40], such as electric cell-substrate impedance sensing systems (40 minutes) and multi-microelectrode arrays (up to 24 hours). Moreover, the PECB enabled the recording of IAPs with higher amplitude and higher SNR, which provided richer details of action potentials, facilitating a deeper exploration of the effects of bitter substances. These findings suggest that PECB provides a simple, easy-to-fabricate, and high-throughput platform for IAPs recordings with more applications for exploring the therapeutic potential of ectopic bitter receptors. However, unlike three-dimensional nanostructured devices, which provide uniform electric fields for electroporation, planar electrodes generate exponentially decaying electric fields[41]. This limitation leads to diminished electroporation efficiency and reduced duration for recording IAPs. Future advancements in our platform could be achieved by integrating three-dimensional microscale and nanoscale electrode designs to enhance intracellular resolution. On the other hand, the HL-1 cardiomyocyte cell line provides a stable and reproducible model for investigating the effects of ectopically expressed bitter receptors on cardiomyocytes. However, it does not fully replicate the electrophysiological behavior of human cardiomyocytes. Future studies will employ human-induced pluripotent stem cell-derived cardiomyocytes (hiPSC-CMs) to validate the findings in more clinically relevant conditions[42]. Although this study underscores the potential signaling pathways and therapeutic implications involving ectopic bitter receptors, further investigation employing molecular biology techniques and patch-clamp analysis is necessary to confirm the exact mechanisms[43].

Conclusion

In this study, we developed a PECB to investigate the therapeutic potential of ectopic bitter receptors in cardiomyocytes. The PECB facilitates a straightforward, efficient, and high-throughput recording of IAPs in cardiomyocytes while maintaining excellent biocompatibility. Utilizing this platform, we examined the potential therapeutic effects of three bitter substances (diphenidol, denatonium benzoate, and arbutin) and found that arbutin effectively alleviated the LQTS. This therapeutic effect may be due to arbutin's activation of bitter receptors, which modulates Ca^{2+} dynamics and potentially

reduces cardiomyocyte repolarization time. The PECB may provide a new tool for heart disease drug screening. However, the exponentially decaying electric fields of planar electrodes limit electroporation efficiency, and HL-1 cells do not fully mimic human cardiomyocytes. This highlights the necessity for future enhancements, such as integrating three-dimensional micro-nanoscale electrodes, the use of hiPSC-CMs, and the implementation of molecular-level validations.

Acknowledgements
This work was supported by the National Key Research and Development Program of China (2024YFB3212300), Key Project of Zhejiang Province (2023C03104, 2024C03146), National Natural Science Foundation of China (32201082, 62301481, 62401505), Scientific Research Fund of Zhejiang Provincial Education Department (Y202353232), the Postdoctoral Fellowship Program of CPSF (GZC20232333), Postdoctoral Science Foundation Funded Project (BX2021265, 2021M702859), the Fundamental Research Funds for the Central Universities (226-2024-00059).

Author details
[1]Biosensor National Special Laboratory, Key Laboratory for Biomedical Engineering of Education Ministry, Department of Biomedical Engineering, Zhejiang University, Hangzhou 310027, China. [2]The MOE Frontier Science Center for Brain Science & Brain-Machine Integration, Zhejiang University, Hangzhou 310027, China. [3]Cancer Center, Binjiang Institute of Zhejiang University, Hangzhou 310027, China. [4]General Surgery Department, Children's Hospital, Zhejiang University School of Medicine, National Clinical Research Center for Child Health, Hangzhou 310052, China. [5]State Key Laboratory of Advanced Drug Delivery and Release Systems, College of Pharmaceutical Sciences, Zhejiang University, Hangzhou 310058, China. [6]The State Key Lab of Brain-Machine Intelligence, Zhejiang University, Hangzhou 310027, China

Conflict of interest
P.W. is an Editor for the journal, no other author has reported any competing interest.

Supplementary information The online version contains supplementary material available at https://doi.org/10.1038/s41378-025-00985-5.

Received: 17 March 2025 Revised: 21 May 2025 Accepted: 23 May 2025
Published online: 04 August 2025

References

1. Yarmolinsky, D. A., Zuker, C. S. & Ryba, N. J. P. Common sense about taste: from mammals to insects. *Cell* **139**, 234–244 (2009).
2. Luo, X. C. et al. Infection by the parasitic helminth activates a Tas2r-mediated signaling pathway in intestinal tuft cells. *Proc. Natl. Acad. Sci. USA* **116**, 5564–5569 (2019).
3. Tizzano, M., Cristofoletti, M., Sbarbati, A. & Finger, T. E. Expression of taste receptors in Solitary Chemosensory Cells of rodent airways. *BMC Pulm. Med.* **11**, 1–12 (2011).
4. Flegel, C., Manteniotis, S., Osthold, S., Hatt, H. & Gisselmann, G. Expression profile of ectopic olfactory receptors determined by deep sequencing. *PLoS ONE* **8**, e55368 (2013).
5. Depoortere, I. Taste receptors of the gut: emerging roles in health and disease. *Gut* **63**, 179–190 (2014).
6. Lee, S. J., Depoortere, I. & Hatt, H. Therapeutic potential of ectopic olfactory and taste receptors. *Nat. Rev. Drug Discov.* **18**, 116–138 (2019).
7. Ma, J. Y. et al. High purity human-induced pluripotent stem cell-derived cardiomyocytes: electrophysiological properties of action potentials and ionic currents. *Am. J. Physiol. Heart C.* **301**, H2006–H2017 (2011).
8. Duncan, G. et al. Drug-mediated shortening of action potentials in LQTS2 human induced pluripotent stem cell-derived cardiomyocytes. *Stem Cells Dev.* **26**, 1695–1705 (2017).
9. Tanwar, A., Gandhi, H. A., Kushwaha, D. & Bhattacharya, J. A review on microelectrode array fabrication techniques and their applications. *Mater. Today Chem.* **26**, 101153 (2022).
10. Conant, G. et al. High-content assessment of cardiac function using heart-on-a-chip devices as drug screening model. *Stem Cell Rev. Rep.* **13**, 335–346 (2017).
11. Zhou, J. et al. Implantable electrochemical microsensors for in vivo monitoring of animal physiological information. *Nano Micro Lett.* **16**, 49 (2024).
12. Xie, C., Lin, Z. L., Hanson, L., Cui, Y. & Cui, B. X. Intracellular recording of action potentials by nanopillar electroporation. *Nat. Nanotechnol.* **7**, 185–190 (2012).
13. Xu, D. X. et al. Scalable nanotrap matrix enhanced electroporation for intracellular recording of action potential. *Nano Lett.* **22**, 7467–7476 (2022).
14. Dipalo, M. et al. Plasmonic meta-electrodes allow intracellular recordings at network level on high-density CMOS-multi-electrode arrays. *Nat. Nanotechnol.* **13**, 972–972 (2018).
15. Dagan-Wiener, A. et al. BitterDB: taste ligands and receptors database in 2019. *Nucleic Acids Res.* **47**, D1179–D1185 (2019).
16. Itzhaki, I. et al. Modelling the long QT syndrome with induced pluripotent stem cells. *Nature* **471**, 225–229 (2011).
17. Pan, Y. X. et al. A hand-held optoelectronic tongue for the identification of heavy-metal ions. *Sens. Actuat. B. Chem.* **352**, 130971 (2022).
18. Lin, Z. C. et al. Accurate nanoelectrode recording of human pluripotent stem cell-derived cardiomyocytes for assaying drugs and modeling disease. *Microsyst. Nanoeng.* **3**, 1–7 (2017).
19. Spira, M. E. & Hai, A. Multi-electrode array technologies for neuroscience and cardiology. *Nat. Nanotechnol.* **8**, 83–94 (2013).
20. Seibertz, F. et al. A modern automated patch-clamp approach for high throughput electrophysiology recordings in native cardiomyocytes. *Commun. Biol.* **5**, 969 (2022).
21. Hu, N. et al. Intracellular recording of cardiomyocyte action potentials by nanobranched microelectrode array. *Biosens. Bioelectron.* **169**, 112588 (2020).
22. Foster, S. R. et al. Bitter taste receptor agonists elicit G-protein-dependent negative inotropy in the murine heart. *FASEB J.* **28**, 4497–4508 (2014).
23. D'Urso, O. & Drago, F. Pharmacological significance of extra-oral taste receptors. *Eur. J. Pharm.* **910**, 174480 (2021).
24. Freund, J. R. et al. Activation of airway epithelial bitter taste receptors by Pseudomonas aeruginosa quinolones modulates calcium, cyclic-AMP, and nitric oxide signaling. *J. Biol. Chem.* **293**, 9824–9840 (2018).
25. Welcome, M. O., Dogo, D. & Mastorakis, N. E. Cellular mechanisms and molecular pathways linking bitter taste receptor signalling to cardiac inflammation, oxidative stress, arrhythmia and contractile dysfunction in heart diseases. *Inflammopharmacology* **31**, 89–117 (2023).
26. Xie, C. et al. Role of intestinal bitter sensing in enteroendocrine hormone secretion and metabolic control. *Front. Endocrinol.* **9**, 576 (2018).
27. Bloxham, C. J., Foster, S. R. & Thomas, W. G. A bitter taste in your heart. *Front. Physiol.* **11**, 431 (2020).
28. Yuan, G. Y., Jing, Y., Wang, T., Fernandes, V. S. & Xin, W. K. The bitter taste receptor agonist-induced negative chronotropic effects on the Langendorff-perfused isolated rat hearts. *Eur. J. Pharm.* **876**, 173063 (2020).
29. Mandel, W. J. et al. Diphenidol: a new agent for the treatment of digitalis-induced arrhythmias electrophysiologic and hemodynamic studies. *Am. J. Cardiol.* **30**, 67–73 (1972).
30. Leung, Y. M., Wu, B. T., Chen, Y. C., Hung, C. H. & Chen, Y. W. Diphenidol inhibited sodium currents and produced spinal anesthesia. *Neuropharmacology* **58**, 1147–1152 (2010).
31. Wei, X. W. et al. Hybrid integrated cardiomyocyte biosensors for bitter detection and cardiotoxicity assessment. *ACS Sens.* **6**, 2593–2604 (2021).
32. Nalban, N. et al. Arbutin attenuates isoproterenol-induced cardiac hypertrophy by inhibiting TLR-4/NF-κB pathway in mice. *Cardiovasc. Toxicol.* **20**, 235–248 (2020).
33. Asakura, K. et al. Improvement of acquisition and analysis methods in multi-electrode array experiments with iPS cell-derived cardiomyocytes. *J. Pharmacol. Toxicol. Methods* **75**, 17–26 (2015).
34. Himmel, H. M. et al. Field and action potential recordings in heart slices: correlation with established in vitro and in vivo models. *Br. J. Pharm.* **166**, 276–296 (2012).

35. Hayes, H. B. et al. Novel method for action potential measurements from intact cardiac monolayers with multiwell microelectrode array technology. *Sci. Rep.* **9**, 11893 (2019).
36. Garg, P. Precision medicine in cardiac channelopathy: integrating genome editing and induced pluripotent stem cells to decipher variant of unknown significance. *Circ. Res.* **123**, A256 (2018).
37. Zhang, F. et al. Activation of PKC affects the ventricular restitution properties and arrhythmogenesis through L-type Ca current. *Pace* **47**, 1131–1140 (2024).
38. Gu, Q., Joe, D. S. & Gilbert, C. A. Activation of bitter taste receptors in pulmonary nociceptors sensitizes TRPV1 channels through the PLC and PKC signaling pathway. *Am. J. Physiol. Lung C.* **312**, 1326–1333 (2017).
39. Bounous, H., Cagin, N., Levitt, B. & Somberg, J. The effect of diphenidol on ouabain cardiotoxicity in the cat. *Br. J. Pharmacol.* **63**, 73 (1978).
40. Qin, C. L. et al. A bioinspired in vitro bioelectronic tongue with human T2R38 receptor for high-specificity detection of N-C = S-containing compounds. *Talanta* **199**, 131–139 (2019).
41. Lu, K. Y. et al. Three dimensional electrode array for cell lysis via electroporation. *Biosens. Bioelectron.* **22**, 568–574 (2006).
42. Wells, S. P. et al. Cardiomyocyte functional screening: interrogating comparative electrophysiology of high-throughput model cell systems. *Am. J. Physiol. Cell Physiol.* **317**, C1256–C1267 (2019).
43. Verkerk, A. O. et al. Patch-clamp recording from human induced pluripotent stem cell-derived cardiomyocytes: improving action potential characteristics through dynamic clamp. *Int. J. Mol. Sci.* **18**, 1873 (2017).